Award Number:
W81XWH-08-1-0609

TITLE:
Experimental Analysis and Computational Modeling of Network
States and Drug Responses in the PI3K/Akt/mTOR Network

PRINCIPAL INVESTIGATOR:
John Albeck

CONTRACTING ORGANIZATION:
Harvard Medical School
Boston, MA 02115

REPORT DATE:
September 2010

TYPE OF REPORT:
Annual summary

PREPARED FOR: U.S. Army Medical Research and Materiel Command
               Fort Detrick, Maryland 21702-5012

DISTRIBUTION STATEMENT: (Check one)

     x Approved for public release; distribution unlimited

REPORT DOCUMENTATION PAGE

Public reporting burden for this collection of information is estimated to average 1 hour per response, including the time for reviewing instructions, searching existing data sources, gathering and maintaining the data needed, and completing and reviewing this collection of information. Send comments regarding this burden estimate or any other aspect of this collection of information, including suggestions for reducing this burden to Department of Defense, Washington Headquarters Services, Directorate for Information Operations and Reports (0704-0188), 1215 Jefferson Davis Highway, Suite 1204, Arlington, VA 22202-4302. Respondents should be aware that notwithstanding any other provision of law, no person shall be subject to any penalty for failing to comply with a collection of information if it does not display a currently valid OMB control number. **PLEASE DO NOT RETURN YOUR FORM TO THE ABOVE ADDRESS.**

1. REPORT DATE *(DD-MM-YYYY)*	2. REPORT TYPE	3. DATES COVERED *(From - To)*
30-09-2010	Annual Summary	1 SEP 2009 - 31 AUG 2010

4. TITLE AND SUBTITLE	5a. CONTRACT NUMBER
Experimental Analysis and Computational Modeling of Network States and Drug Responses in the PI3K/Akt/mTOR Network	
	5b. GRANT NUMBER
	W81XWH-08-1-0609
	5c. PROGRAM ELEMENT NUMBER

6. AUTHOR(S)	5d. PROJECT NUMBER
John Albeck	
	5e. TASK NUMBER
Email: john_albeck@hms.harvard.edu	
	5f. WORK UNIT NUMBER

7. PERFORMING ORGANIZATION NAME(S) AND ADDRESS(ES)	8. PERFORMING ORGANIZATION REPORT NUMBER
Harvard Medical School Boston MA 02115-6027	

9. SPONSORING / MONITORING AGENCY NAME(S) AND ADDRESS(ES)	10. SPONSOR/MONITOR'S ACRONYM(S)
U.S. Army Medical Research And Materiel Command	
	11. SPONSOR/MONITOR'S REPORT NUMBER(S)

12. DISTRIBUTION / AVAILABILITY STATEMENT
Approved for public release; distribution unlimited

13. SUPPLEMENTARY NOTES

14. ABSTRACT
In breast cancer, the PI3K/Akt/mTOR and Ras/MEK/ERK signaling networks are believed to play a critical role in controlling tumor proliferation and survival, and thus are the main targets for a range of signaling inhibitors currently in clinical use or undergoing clinical trials. To make the most effective use of these inhibitors, we are developing quantitative models to predict inhibitor efficacy for individual patients based on the unique signaling states of the Akt and ERK networks. In the current report, we describe our identification of the cell cycle inhibitor p57^{Kip2} as a novel integration point between the ERK and Akt networks, and characterized the dynamics of p57^{Kip2} regulation in response to PI3K network activation in mammary epithelial cells. We also describe a newly constructed cell system for simultaneously measuring signaling and proliferation in real time in living cells. Data collected from this system are now being used to extend and refine our computational models.

15. SUBJECT TERMS
None provided

16. SECURITY CLASSIFICATION OF:			17. LIMITATION OF ABSTRACT	18. NUMBER OF PAGES	19a. NAME OF RESPONSIBLE PERSON USAMRMC
a. REPORT U	**b. ABSTRACT** U	**c. THIS PAGE** U	UU	30	**19b. TELEPHONE NUMBER** *(include area code)*

Table of Contents

Introduction

Central to the development of cancer therapies targeting signal transduction pathways is a detailed understanding of how such pathways control cell behavior. Much is now known about proteins like Ras, ErbB2, and Akt that, when hyperactivated, drive hyperproliferation and unwarranted cell survivial, but two key aspects of these pathways remain ambiguous. First, the process of integrating signals from multiple pathways to make cellular phenotypic decisions is poorly understood. While a number of integration mechanisms have been identified, there are likely many more that remain unknown. Furthermore, the net effect of these signal integration mechanisms, and how they sum to determine cell fate, remains uncertain. Second, the quantitative relationship between flux through signaling networks and cellular phenotype, while key to the concept that reducing such flux via inhibitors will have a beneficial effect, remains unexplored. The dearth of studies addressing this second problem area can largely be attributed to technical hurdles – because signals and phenotypes vary from cell to cell and over time, measurements of both must be made simultaneously at the single cell level and must be both quantitative and dynamic.

My work over the past year has led to insights into both problems. In the first area, our high-throughput survey of signaling dynamics in the PI3K pathway has led us to identify a novel integration point between the PI3K/Akt/mTOR and Ras/Raf/Erk pathways controlling cell cycle commitment. In the second problem area, I have developed a new live-cell reporter system that enables us to dynamically link signaling flux in the PI3K and Erk pathways to cellular proliferation across multiple generations of proliferating cells. This system is now providing an unprecedented real-time view of the signaling events controlling proliferation. The data collected are currently being used to construct detailed computational models relating signaling and proliferation, with the goal of predicting the phenotypic effects of targeted signaling inhibitors that are now in clinical use.

Body

Materials and Methods

Cell lines and constructs
All plasmids described herein were constructed in the retroviral vectors pBabe or pMSCV using standard PCR and molecular cloning techniques. All cell lines were derived from MCF-10A mammary epithelial cells. Reporters and other constructs were introduced and stably integrated using retroviral particles generated in 293T cells using pCL-Eco or pCL-Ampho. Clonal derivatives of reporter lines were isolated by limiting dilution in 96-well plates followed by screening to identify clones with appropriate expression levels and epithelial morphology similar to the parental line.

High-throughput immunofluorescence microscopy
Cells were cultured in optical plastic 96-well plates (Corning #3603) and treated with growth factors and inhibitors as indicated. Fixation was in 2% formaldehyde, followed by permeabilization in 100% methanol at -20 C. Blocking and incubation with primary/secondary antibodies was performed in Odyssey blocking buffer (LICOR). Primary antibodies were obtained from Cell Signaling, BD Biosciences, and Santa Cruz Biotechnology, and Alexa fluor 488-, 555-, or 647-conjugated secondary antibodies were obtained from Invitrogen. Data were collected using an Applied Precision Cellworx scanner in the Institute for Chemistry and Cell Biology at Harvard Medical School.

Live-cell microscopy
Cells were cultured on collagen-coated #1.5 glass-bottom 96- (Matrical), 6-, or 24-well plates (MatTek) in DMEM/F12 lacking phenol red. Time-lapse imaging was performed on Perfect Focus System-equipped Nikon TE2000 or Ti microscopes fitted with environmental chambers using 10x or 20x objective lenses. Images were

4

collected at 20 or 30 minute intervals for up to 180 stage postions per plate. When appropriate, medium was changed at 24-hour intervals to prevent depletion of growth factors or inhibitors.

Computational analysis of microscope data
Image segmentation and analysis was performed in Matlab using routines derived from CellProfiler (Lamprecht, Sabatini et al. 2007). Reporter signals were calculated as mean pixel intensities for segmented regions following rolling ball background subtraction. Tracking of cells was performed manually or using published algorithms (Jaqaman, Loerke et al. 2008).

Computational modeling
Agent-based computational models of proliferation were implemented in Matlab based on a transition probability framework (Smith and Martin 1973). Rule-based models were constructed using the kappa modeling language and simulated in Cellucidate/Rulebase.

Results

I discuss here results obtained over the past 12 months in relation to the current Statement of Work. For reference, the experiments proposed in the SOW are shown in italics.

***Specific Aim 1. Collect a comprehensive single-cell dataset of PI3K network states and cellular responses.** A large scale systematic data set will be collected, monitoring multiple signaling proteins over time in response to growth factors, small molecule inhibitors, and oncogene expression. High-throughput microscopy will be used to measure both protein network signals and cellular responses.*

a. Pilot study to optimize perturbations, doses, cell lines, time points, and serum conditions. (Months 1-3.)

b. Identify antibodies and optimize plating conditions for high throughput immunofluorescence microscopy (HTIF). (Months 3-9)

c. Perform HTIF analysis of time-course behavior, monitoring proteins in the PI3K network (including antibodies against pAkt, pS6, c-Myc, c-Jun, Fra-1, CyclinD1/2/3, $p21^{Cip1}$, $p27^{Kip1}$, $p57^{Kip2}$ (Months 9-12)

d. Segmentation of images and quantitative analysis of data using computational routines. (Months 9-12)

Aims 1a-1d have been completed, as detailed in my year 1 annual report. Over the past year (months 13-24), analysis of the resulting data set has led to the generation of a hypothesis concerning the role of the cell cycle inhibitor $p57^{Kip2}$ in controlling PI3K/Akt-driven proliferation. In the initial data set, expression of p57 increased under conditions of high PI3K/Akt signaling (insulin/IGF stimulation), but decreased under conditions of strong Erk signaling (EGF stimulation). Because mammary epithelial cells display only a weak proliferative response to IGF, but proliferate rapidly in respone to EGF, we hypothesized that the upregulation of p57 by the PI3K/Akt pathway may be a key factor in limiting the response to IGF. Extensive testing using p57 knockdown, overexpression of various oncogenes, and pharmacological inhibition provided strong support for this hypothesis. Additionally, we found that depletion of p57 synergized strongly with mutation of the PI3K p110a subunit to enable proliferation, indicating that p57 can serve as a key endogenous barrier to transformation of epithelial cells by hyperactivation of the PI3K pathway. These findings provide a strong rationale for the finding that p57 is lost in many breast cancers (Yang, Karuturi et al. 2009), and may also explain why many cancers with PI3K mutation also acquire Erk-activating mutations, which would counteract the Akt-mediated upregulation of p57. The status of p57 expression may thus be a factor in predicting the response of tumors to PI3K-targeted therapy, a possibility we are currently investigating. A manuscript describing this portion of the study will be submitted for publication shortly, and is attached as an appendix.

e. Collect data on cellular responses to PI3K activation and inhibition using live cell microscopy to monitor cell proliferation, cell death, and motility. (Months 12-20)

I have now optimized long-term live-cell microscopy for MCF-10A cells and have collected several data sets in which thousands of individual cells expressing various fluorescent constructs have been followed over the course of 72-96 hours under various growth factor and signaling inhibitor concentrations. In this system, the primary responses to growth factors and signaling inhibitors are changes in proliferation and motility, rather than cell death, and I have thus chosen to focus on proliferation as the readout most likely to reflect in vivo effectiveness of signaling inhibition. However, in future work I plan to examine cell death in response to PI3K pathway inhibitors in combinations with other inhibitors that others in our group have shown to be effective at inducing cell death. To provide a live-cell proliferation readout, I have adapted a published cell cycle reporter (Sakaue-Sawano, Kurokawa et al. 2008) that marks the induction of S-phase (Fig. 1), using the red fluorescent protein mCherry. To facilitate both long-term cell tracking and computational segmentation of individual cells, I have combined this reporter in a bicistronic retroviral vector with a nuclear localized mCerulean (a cyan fluorescent protein). One initial challenge in developing cell lines using this reporter system was variability in reporter expression due to integration site effects; this was overcome by isolating multiple clones and identifying those with stable, homogenous expression at levels high enough to enable microscopic detection, but not high enough to perturb cellular function. Effects of growth factors and inhibitors on proliferation occur on the order of 1-3 days, while most current live-cell experiments span 1-24 hours, and we thus optimized conditions to allow extended data collection. An imaging interval of 20 minutes was found to be sufficiently frequent to capture high-resolution data for cell cycle events, but infrequent enough to avoid all evidence of phototoxicity. This imaging frequency also permitted up to 160 individual stage positions to be imaged within each experiment, allowing data collection for multiple conditions and replicates within a multi-well plate for each experiment. An additional challenge in collecting data for several days was depletion of growth factors or inhibitors from the culture medium; this problem was overcome by growing a smaller number of cells within a larger (24-well) plate, enabling an excess volume of medium to be used (to maintain cell density, cells were patterned within a small collagen-coated spot at the center of each well.

Because each movie contains hundreds of cell lineages, and each lineage 5-20 cell division events, data analysis and annotation are the largest challenge associated with this method. Using a combination of published computational methods (Jaqaman, Loerke et al. 2008; Carpenter 2009), it is now possible to extract both population-level and individual cell metrics. However, the tracking process remains error-prone, requiring significant manual intervention to accurately assemble complete lineages, and optimization of this process is ongoing.
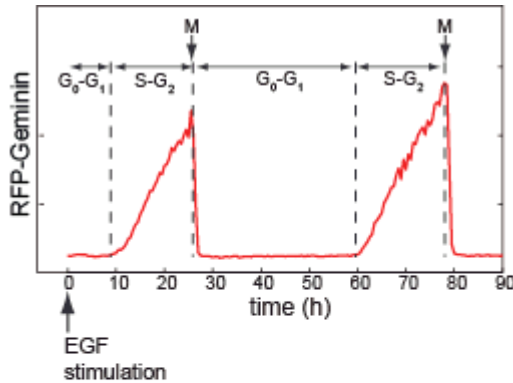
Figure 1. Tracking of cell cycle progression in an individual mammary epithelial cell. MCF-10A cells expressing an RFP-Geminin fusion protein were cultured in the absence of EGF for 2 days and re-stimulated with EGF at time 0. The RFP fluorescence for one cell is shown with the corresponding cell cycle phases labeled.
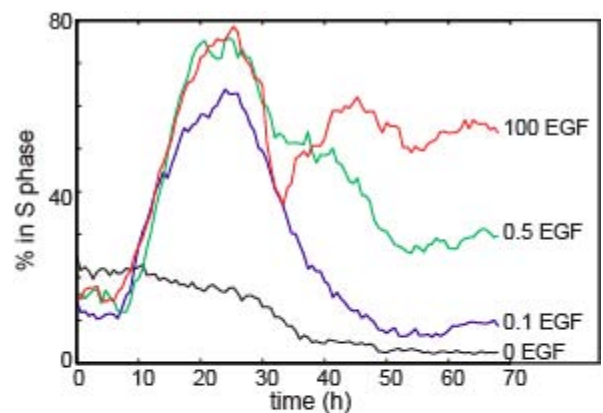
Figure 2. Real-time tracking of proliferation in populations of cells. MCF-10A cells expressing an RFP-Geminin fusion protein were cultured in the absence of EGF for 2 days and re-stimulated with EGF at time 0. The percent of cells positive for RFP fluorescence is shown as a function of time.
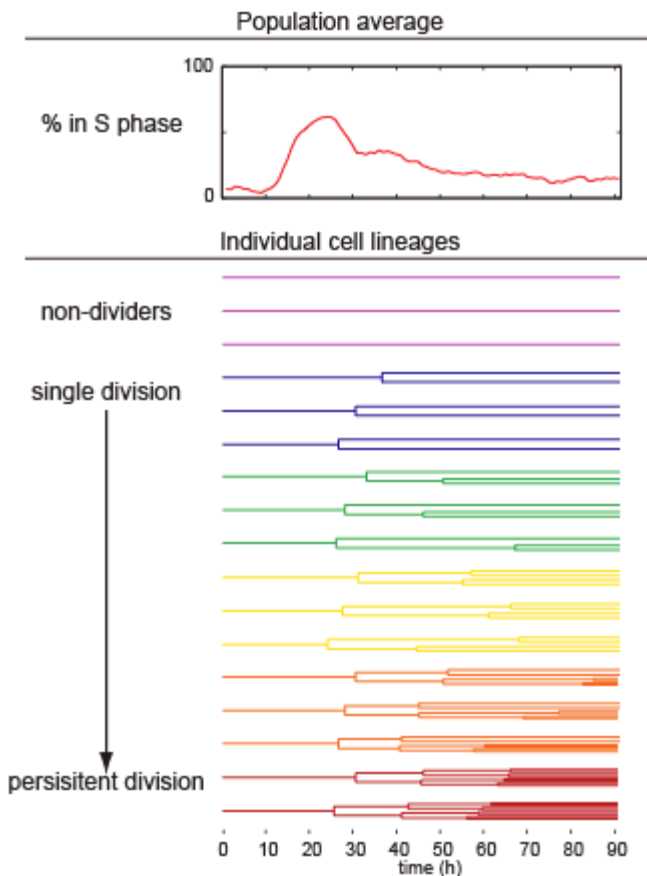
6

Figure 3. Tracking of cell lineages in response to EGF. MCF-10A cells expressing an RFP-Geminin fusion protein were cultured in the absence of EGF for 2 days and re-stimulated with 0.5 ng/ml EGF at time 0. At top, the percent of cells positive for RFP fluorescence is shown as a function of time. At bottom, individual lineages are plotted with each cell division is represented as a branching event.

Using this real-time imaging system, I have now collected data on cells responding to growth factors following a period of withdrawal, and cells responding to various signal transduction inhibitors. Analysis of these data has found much that is consistent with previous work on cell cycle control using older methods, but has also revealed a number of new features that will require significant updates to existing models of cell cycle control. As observed previously, re-entry into S-phase begins 10-12 hours following re-stimulation with growth factor, with most cells in the population($\sim$80%) beginning S-phase semi-synchronously (Fig. 2). The timing of this first wave of cell cycle re-entry is insensitive to the concentration of EGF present, but the fraction of cells participating varies, with more cells re-entering at higher concentrations. Following this first wave of proliferation, synchronicity is lost, and a dynamic equilibrium of "steady-state" proliferation is established, in which the fraction of cells in S-phase remains constant as individual cells continue to cycle (Fig. 2). Strikingly, analysis of cell lineages during this process reveals a pronounced "memory effect", in which certain cell lineages divide repeatedly with a cycle time of <15 hours, while other cells display cycle times >30 hours or fail to divide at all (Fig. 3). Thus, accurate modeling of the proliferative response to EGF signaling will need to incorporate signaling states that persist across multiple cell generations.

Signaling pathways are thought to control the cell cycle prior to the so-called "restriction point" in late G_1 phase, at which time commitment to the cell cycle becomes independent of growth factor stimulation (Pardee 1974). Consistent with this model, withdrawal of EGF from cycling MCF-10A cells resulted in a G_0/G_1 arrest; cells that were mCherry-geminin positive at the time of withdrawal completed mitosis before arresting. However, when EGF signaling was blocked by the addition of the antagonistic antibody C225 or the small molecule EGFR kinase inhibitor gefitinib, a large number ($\sim$50%) of mCherry-geminin-positive cells exited the cycle immediately and became mCherry-geminin-negative without dividing. Given the different mechanisms of action of these two inhibitors, it is highly unlikely that this effect is due to off-target effects. Moreover, the suppression of proliferation by these two inhibitors was much more effective than that induced by EGF withdrawal alone. Together, these data indicate that continual EGF signaling is required to maintain cell cycle progression; the tendency of cells to progress to G_0/G_1 upon EGF withdrawal is likely a result of residual signaling or ongoing autocrine stimulation of the EGF receptor. Thus, the standard restriction point model is
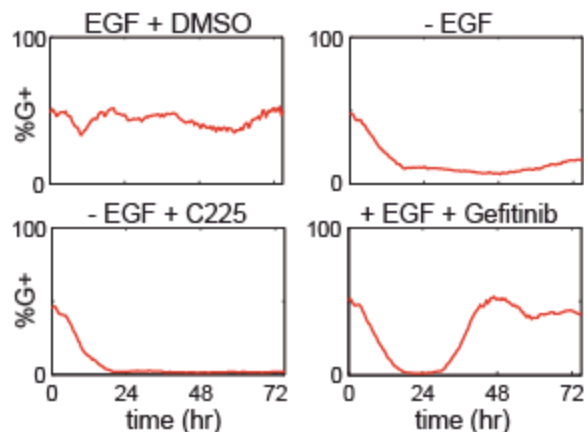

Figure 4. Real-time tracking of proliferation in response to loss of EGF signaling. MCF-10A cells expressing an RFP-Geminin fusion protein were cultured in full growth medium and transferred to the indicated treatments at time 0.

7

insufficient to explain the proliferative behavior of mammary epithelial cells stimulated by EGF.

Treatment of MCF-10A cells with inhibitors of PI3K and mTOR also led to potent inhibition of proliferation, as well as exit of geminin-positive cells from the cell cycle prior to mitosis (Fig. 5). A feature observed with all small molecule signaling inhibitors was loss of effectiveness after ~48 hours. In the case of gefitinib, where the loss is most pronounced, this effect is due to breakdown of the inhibitor, as re-addition of fresh inhibitor at 24 hour intervals prevents the re-initiation of proliferation. I am currently testing whether the other inhibitors lose their effectiveness over time due to inhibitor breakdown or due to network adaptation.
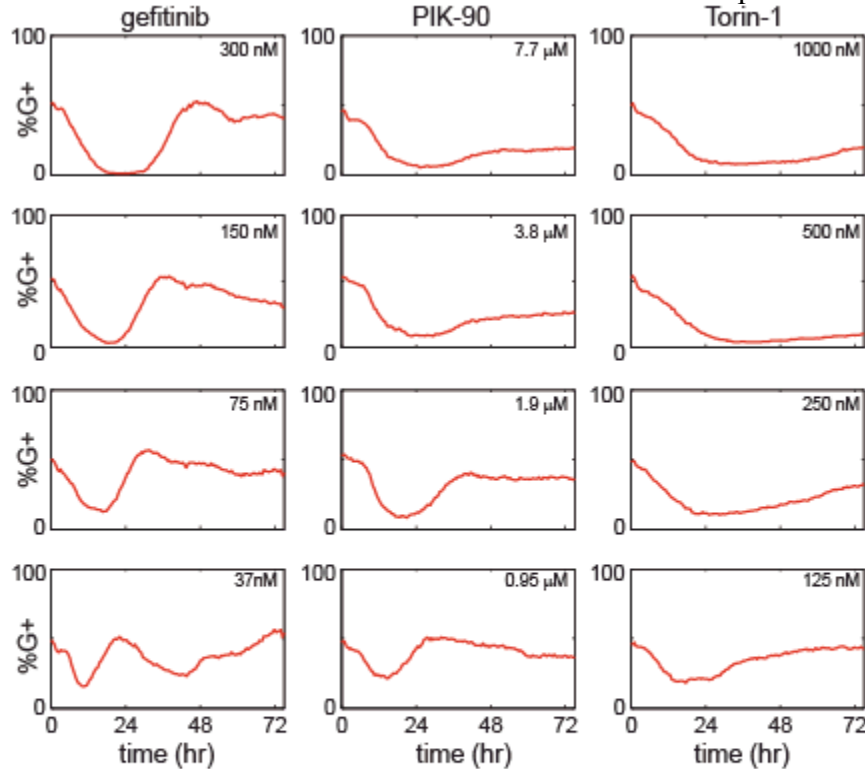

Figure 5. Real-time tracking of proliferation in response to signaling pathway inhibitors. MCF-10A cells expressing an RFP-Geminin fusion protein were cultured in full growth medium and treated with the indicated concentrations of inhibtors at time 0.

*2. **Develop an integrated predictive model of proliferative responses to PI3K pathway inhibitors.** Prototype models will first be constructed based on data collected in Aim 1. Further model development will be performed concurrently with data collection as described in Aim 3. The function and output of the PI3K network will be modeled at both the molecular and cellular scale and calibrated using experimental data.*

a. Generate agent-based model of network states and cell responses collected in Aim 1. (Months 1-12)

b. Develop a mechanistic model of the PI3K pathway using rule-based modeling language. (Months 1-12)

As discussed in the previous annual report, prototypes for models in a) and b) were developed during months 1-12.

c. Update and expand models using data collected in Aim 3. (Months 12-30)

Progress on model development has continued as additional data become available. As illustrated in Fig. 6, the rule-based mechanistic model of the core Akt activation network has been calibrated to fit data generated under
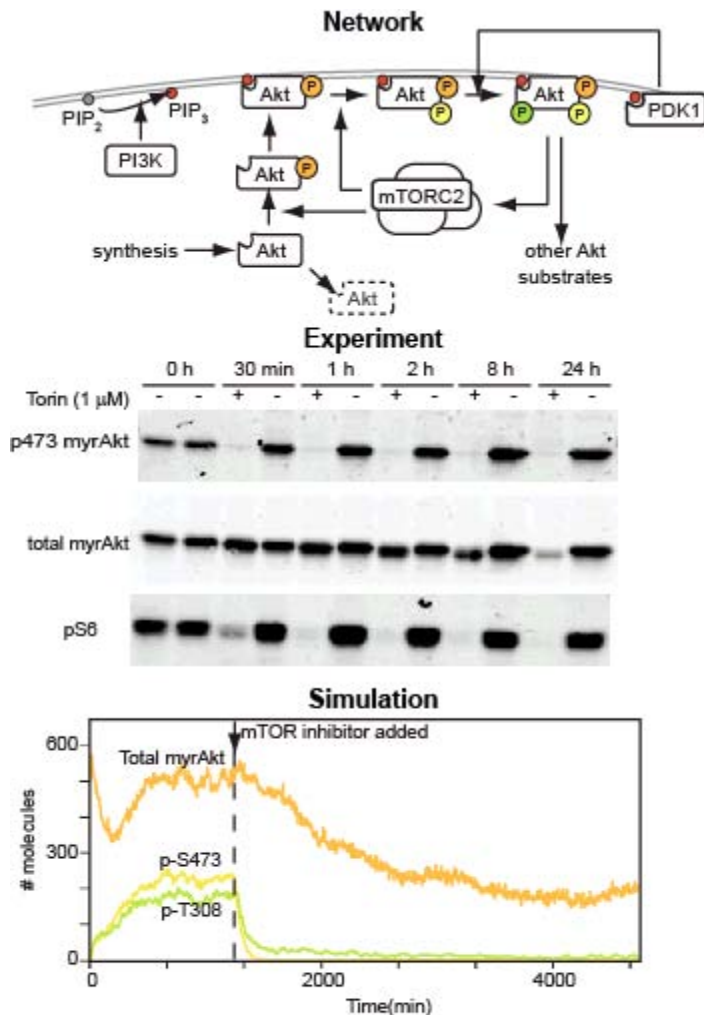
Figure 6. Calibration of a core Akt activation model. Top, topology of the modeled network. Middle, experimental data corresponding to the network shown. Bottom, stochastic simulation of the network model.

Aim 3. Our core model includes the dual positive feedback loop between Akt and mTORC-2 identified during the first year of the project. Simulation of mTOR kinase inhibition with this model accurately recapitulates both the rapid loss of phosphorylation at Ser-473 and the slow decrease in Akt expression observed experimentally (Fig. 6). We are continuing to extend this model to include other known feedback loops impinging on Akt activation.

In the case of the agent-based model, our current prototype successfully captures the memory effect observed by live-cell microscopy, because progeny cells in the model inherit their signaling state upon cell division. However, the initial model was based on a restriction point framework, in which proliferation decisions were controlled by signaling only during early G_1 phase. To accurately capture the responses to pharmacological inhibition observed by live cell microscopy (see Aim 1), I am in the process of re-formulating the model to enable modeled cells to exit the cell cycle upon signaling inhibition. It will thus be important to determine the extent of hysteresis in the decision process; that is, are the levels of signals required to maintain cell cycle progression lower than the levels needed to initially commit to cell cycle entry? This question will be answered through detailed analysis of the live-cell data described in Aims 1 and 3.

d. Generate an integrated multiscale model by embedding rule-based mechanistic network model within the agent-based cellular model. Simulate population growth under varying conditions of PI3K pathway activation and inhibition. (Months 25-30)

As data become available from the live-cell reporters described in Aim 3, work on an integrated model is now being initiated.

3. Collect molecularly detailed data for model parameterization and test model predictions. *Directed experimental analysis will provide additional data for model building and testing.*

a. Generate mutant Akt constructs and analyze pathway activation and feedback regulation in isolation from other growth factor networks. (Months 7-30)

These data were described in detail in the previous annual report. Work has continued using the inducible Akt constructs generated, and has been used to calibrate our mechanistic Akt model as described in Aim 2 above.

b. Generate and test live-cell reporters for PI3K/Akt pathway activity. Reporters will be constructed by fusing fluorescent proteins to domains conferring Akt pathway-regulated stability or localization. (Months 19-24)
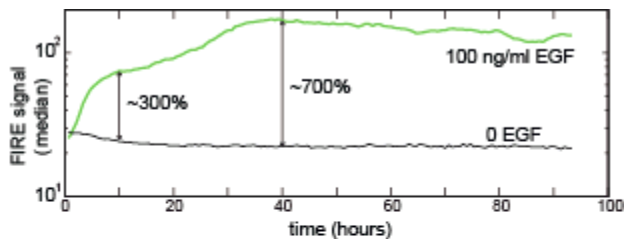
Figure 7. Response characteristics of FIRE. MCF-10A cells expressing FIRE were cultured in the absence of EGF for 2 days and re-stimulated with 100 ng/ml EGF or vehicle at time 0. The population median FIRE signal is plotted as a function of time.

Several approaches have been attempted to develop high-sensitivity reporters suitable for tracking PI3K and related signaling in living cells. Although FRET-based reporters currently dominate the field, my initial work has indicated that these reporters do not provide sufficient sensitivity to detect the signaling events involved in steady-state proliferation in MCF-10A cells. A second reporter strategy that was also implemented was a localization-based reporter based on Foxo3a. Because Foxo1 and Foxo3a translocate from the the nucleus to the cytosol upon phosphorylation by Akt (Brunet, Bonni et al. 1999), GFP fusions to these proteins have been used as readouts for Akt activity (Zanella, Rosado et al. 2008). However, in its simplest form, this strategy has the disadvantage of requiring the overexpression of the growth inhibitory Foxo transcription factors, a problem that can in principle be overcome by engineering these proteins to no longer bind DNA or initiate transcription. Based on immunofluorescence data that demonstrated that Foxo3a, but not Foxo1, translocated to the nucleus upon growth factor withdrawal in MCF-10A cells, I focused on Foxo3a as a basis for the reporter. In addition to slower growth, fusions of Foxo3a to YFP also showed highly heterogeneous expression, even within clones. Multiple deletions and point mutations were made, and I identified a fragment comprising residues 1-400 of Foxo3a, in combination with a point mutation in the DNA binding domain (H215R), as the most stably expressed and least growth-inhibitory version. This reporter was expressed at similar levels from cell to cell, and responded to PI3K inhibitors by translocating to the nucleus. However, unlike endogenous Foxo3a, the reporter failed to translocate to the nucleus upon growth factor withdrawal, suggesting that while it is capable of responding to drastic signal changes such as those resulting from pharmacological inhibition, it does not accurately respond to the more subtle changes induced by normal pathway operation. This behavior was shared by all Foxo3a constructs tested, including the full length protein, indicating that this limitation results from some aspect of reporter overexpression. I am attempting to further improve on the current design.

A third strategy for reporter construction and the most successful thus far, is based on protein stability regulation. This approach, in which a protein domain responsible for controlling the degradation rate of an endogenous protein is fused to GFP (or another fluorescent protein), thereby conferring upon GFP the stability characteristics of the endogenous protein, has been used successfully to generate highly sensitive reporters for the cell cycle (Sakaue-Sawano, Kurokawa et al. 2008). However, despite existing knowledge of numerous proteins in which stability is controlled by phosphorylation events, this strategy has not been exploited in kinase signaling pathways. I therefore developed a new set of reporters utilizing the phosphorylation/degradation domains of either c-Myc or members of the c-Fos family. These proteins were chosen as prototypes based on immunofluorescence data collected during year 1 indicating that the levels of these proteins are closely connected to signaling in the PI3K/mTOR network. The stability of c-Myc is controlled by phosphorylation at Ser-62 by Erk and Thr-58 by GSK-3 (Sears, Nuckolls et al. 2000), while the stability of the Fos family is controlled by Rsk/Erk phosphorylation at multiple sites near the C-terminus (Murphy, Smith et al. 2002). These domains were fused to the yellow fluorescent protein mVenus, while in all cases the DNA binding domains were deleted to ensure that reporter expression did not produce phenotypic effects.

Initial testing of the stability-based reporters indicated that they were all capable of responding to EGF-induced signaling. Due to the complexity of dynamics associated with the c-Myc-based reporter (likely a result of the fact that it integrates multiple signals) and a moderate change in cell morphology associated with the c-Fos reporter, I focused for the time being on the reporter based on Fra-1, comprising the C-terminal 108 residues of Fra-1 fused to mVenus. Upon stimulation with EGF, this reporter increased in intensity immediately, reaching a level 3-fold higher than control-treated cells within 10 hours and 7-fold higher at its maximum (Fig. 7).

Figure 8. Computational model of FIRE relative to upstream ERK signaling.

Existing FRET-based reporters of ERK activity show a maximum signal change of 1.2-fold (Harvey, Ehrhardt et al. 2008), suggesting that our strategy provides a >10-fold increase in sensitivity. A simple computational model of the reporter response to pERK explains this increase in sensitivity (Fig. 8); because phosphorylated reporter molecules have an extended half-life, the reporter ac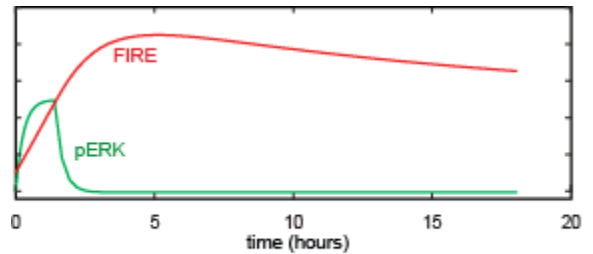ts as an integrator of pERK activity. A small, transient pulse of pERK activity can stabilize a large number of reporter molecules that persist for hours. Thus, the increase in sensitivity requires a tradeoff in response time. However, by using the computational model, it is possible to back-calculate the pERK input that resulted in the observed reporter signal. A second advantage of an integrative reporter is that it does not require frequent time sampling as a more rapidly responding reporter would, allowing for reduced phototoxicity in long-term imaging. Integrative reporters are therefore a better fit for the long-term proliferation tracking that we have put in place (see Aim 1). We refer to the Fra-1-YFP fusion as **F**ra-1-based **I**ntegrative **R**eporter of **E**rk/Rsk (**FIRE**). Efforts are underway to identify the essential features of the Fra-1 fragment for controlling reporter behavior; it appears highly likely that integrative reporters for other kinases can be constructed either by modifying key sequences within FIRE or by fusing other phosphodegron domains to fluorescent proteins.
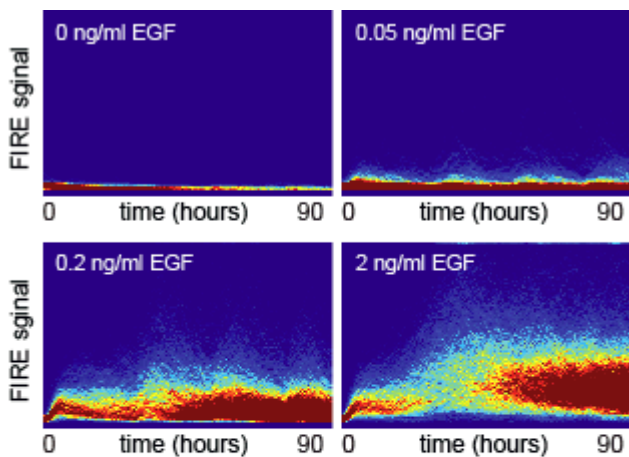

Figure 9. FIRE signal distributions in response to EGF stimulation. MCF-10A cells expressing FIRE were cultured in the absence of EGF for 2 days and re-stimulated with EGF at time 0. The population distribution of FIRE signal intensity is shown as a function of time, where red colors indicate more cells at a given FIRE signal intensity.

c. Real-time single-cell measurements of Akt pathway dynamics in cells growing under conditions of stimulation or pharmacological inhibition. (Months 20-36)

To make these measurements, I have constructed MCF-10A clones stably expressing both the bicistronic NLS-mCerulean/mCherry-Geminin construct and the FIRE reporter. At the population level, stimulation with EGF resulted in a dose-dependent induction of FIRE, while within each dose a broad distribution of response levels were observed (Fig. 9). I am currently analyzing the data to determine how signal strength within each individual cell or cell lineage correlates with the phenotypic behavior of that cell or lineage. Do cells with higher levels proliferate more rapidly or frequently? This question will be addressed by detailed statistical analysis of hundreds of individual cells within the data sets already collected, and will be critical in further developing the agent-based model discussed in Aim 2.

11

I have also made measurements of FIRE signal intensity in response to small molecule inhibitors of EGFR, mTOR, PI3K, or MEK, the kinase upstream of ERK. At the population median level, each of these inhibitors reduced the overall intensity of the FIRE signal (Fig. 10). However, the kinetics of inhibition fell into two classes. For the EGFR and MEK inhibitors, the signal began to decay smoothly immediately following addition of the inhibitor, as would be expected for direct inhibition of the pathway controlling FIRE stability. For PI3K and mTOR inhibitors, the signal loss was less pronounced decayed erratically, as might be expected for inhibition of signals that influence, but are not directly upstream of FIRE. In agreement with this, I have observed by immunofluorescence that inhibition of PI3K or mTOR reduces the ERK activity levels weakly, while direct inhibition of MEK or EGFR strongly blocks ERK activity. Thus, the FIRE reporter can be used to track Erk activity levels in response to inhibition of signaling nodes throughout the network. I am currently analyzing the collected data to determine whether the degree of inhibition, as indicated by the FIRE signal, correlates with phenotypic response (e.g. cell cycle exit).
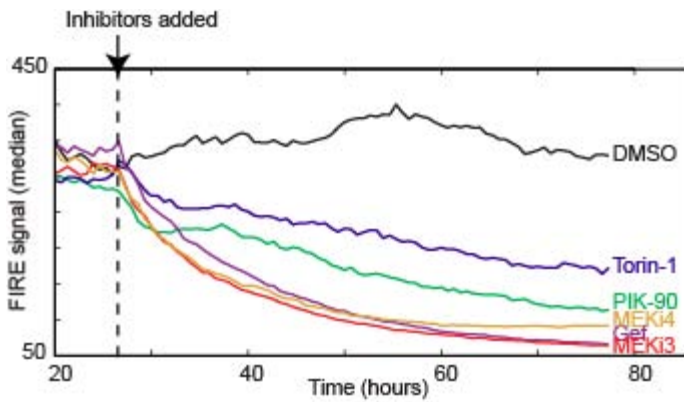

Figure 10. Response of FIRE to signaling inhibitors. MCF-10A cells expressing FIRE were cultured in the presence of 100 ng/ml EGF for 2 days and the indicated inhibitors were added at the indicated time.

d. Test model predictions on 2-3 additional cell lines. (Months 32-36)

These experiments are slated for the coming year and have not yet been initiated

Key research accomplishments

- Identified the cell cycle inhibitor p57^{Kip2} as a key regulator of PI3K-mediated cell proliferation.
- Identified a novel regulatory motif for p57^{Kip2}, in which it is activated by the PI3K pathway and repressed by the ERK pathway.
- Developed a new signaling reporter strategy that enables detection of signaling levels with high sensitivity.
- Determined that inhibition of proliferation-related signaling pathways leads to cell cycle exit in a non-restriction point model.

Reportable outcomes

- The live-cell proliferation assays described herein were used to generate data for a publication (Mazzone, Selfors et al.).
- I presented an abstract and poster at the 2010 International Conference on Systems Biology of Human Disease (abstract attached as an appendix).
- I was invited to apply and subsequently interviewed for a faculty position in the Department of Biomedical Engineering at Cornell University (October 2009) using data collected under this fellowship.

Conclusion

The results presented here advance the overall goals of this research project in two important ways. First, we provide a molecular mechanism for integration of growth signals by the Erk and Akt pathways that helps to explain the disparity in cell proliferation between EGF and IGF-1 mediated signaling. These molecular details can now be integrated into our mechanistic model. Second, we have constructed a unique platform in which signaling dynamics and proliferation can be measured in individual cells over very long periods of time. The

12

data we have collected from this platform are rich sources of information which will allow adaptation and training of the models on large, statistically significant numbers of cells. Thus, the challenge that remains for the final 12 months of this project, in good agreement with the timeline presented in the SOW, is to fully analyze these data sets and use them optimize our existing models. Additional data, including measurements on multiple breast cancer lines responding to inhibitors, will then be used to test the predictiveness of these models.

References

Brunet, A., A. Bonni, et al. (1999). "Akt promotes cell survival by phosphorylating and inhibiting a Forkhead transcription factor." Cell **96**(6): 857-68.

Carpenter, A. E. (2009). "Extracting rich information from images." Methods Mol Biol **486**: 193-211.

Harvey, C. D., A. G. Ehrhardt, et al. (2008). "A genetically encoded fluorescent sensor of ERK activity." Proc Natl Acad Sci U S A **105**(49): 19264-9.

Jaqaman, K., D. Loerke, et al. (2008). "Robust single-particle tracking in live-cell time-lapse sequences." Nat Methods **5**(8): 695-702.

Lamprecht, M. R., D. M. Sabatini, et al. (2007). "CellProfiler: free, versatile software for automated biological image analysis." Biotechniques **42**(1): 71-5.

Mazzone, M., L. M. Selfors, et al. "Dose-dependent induction of distinct phenotypic responses to Notch pathway activation in mammary epithelial cells." Proc Natl Acad Sci U S A **107**(11): 5012-7.

Murphy, L. O., S. Smith, et al. (2002). "Molecular interpretation of ERK signal duration by immediate early gene products." Nat Cell Biol **4**(8): 556-64.

Pardee, A. B. (1974). "A restriction point for control of normal animal cell proliferation." Proc Natl Acad Sci U S A **71**(4): 1286-90.

Sakaue-Sawano, A., H. Kurokawa, et al. (2008). "Visualizing spatiotemporal dynamics of multicellular cell-cycle progression." Cell **132**(3): 487-98.

Sears, R., F. Nuckolls, et al. (2000). "Multiple Ras-dependent phosphorylation pathways regulate Myc protein stability." Genes Dev **14**(19): 2501-14.

Smith, J. A. and L. Martin (1973). "Do cells cycle?" Proc Natl Acad Sci U S A **70**(4): 1263-7.

Yang, X., R. K. Karuturi, et al. (2009). "CDKN1C (p57) is a direct target of EZH2 and suppressed by multiple epigenetic mechanisms in breast cancer cells." PLoS One **4**(4): e5011.

Zanella, F., A. Rosado, et al. (2008). "Chemical genetic analysis of FOXO nuclear-cytoplasmic shuttling by using image-based cell screening." Chembiochem **9**(14): 2229-37.

Proliferation in response to the PI3K/Akt pathway is suppressed by activation of p57[Kip2]

Devin T. Worster[1], Nicole L. Solimini[2], Tobias Schmelzle[3], Bjorn Millard[4], Gordon B. Mills[5], Joan S. Brugge[1], and John G. Albeck[1]

Departments of [1]Cell Biology, [2]Genetics, and [4]Systems biology, Harvard Medical School, Boston, MA
[3]Novartis Pharmaceuticals, Basel, Switzerland
[4]Department of Systems Biology, University of Texas M.D. Anderson Cancer Center, Houston, TX

Abstract

Proliferation of mammary epithelial cells is stimulated by epidermal growth factor (EGF), but not by insulin-like growth factor 1 (IGF-1) or insulin. To understand the signaling mechanisms underlying this difference, we examined a panel of 15 growth-related signaling proteins at the single-cell level using automated high-content immunofluorescence microscopy (HTIF). This analysis revealed that the cell cycle inhibitor p57[Kip2] is highly expressed under conditions of insulin stimulation, but not under EGF. Using a combination of pathway-specific inhibitors and activated signaling proteins, we show that p57[Kip2] is potently activated by Akt activity, but strongly repressed by ERK activity. Depletion of p57[Kip2] enables proliferation in response to insulin alone. Thus, p57[Kip2] is capable of sensing the ratio of ERK- to Akt-mediated signals and arresting cell growth when this ratio is too high. Interestingly, oncogenic mutations in PI3K induce p57[Kip2] expression, and knockdown of p57 potently enhances the proliferative effect of PI3K mutation. Our results offer a potential explanation for the finding that the p57[Kip2] locus is silenced in many breast cancers, which frequently show hyperactivation of the PI3K pathway. The expression status of p57[Kip2] may be an important factor to assess when considering targeted therapy against the ERK or PI3K pathways.

Introduction

In mammalian cells, growth factor-mediated signaling is essential for cellular proliferation and is frequently disrupted in cancer. Activation of growth factor receptors leads to the stimulation of numerous downstream pathways that modulate cellular metabolism, control gene transcription, and engage the cell cycle. Of these pathways, the Ras/Raf/ERK and PI3K/Akt pathways are among the most essential and well-studied. The Ras/Raf/ERK pathway (hereafter the ERK pathway) is typically stimulated by recruitment of guanine nucleotide exchange factors to the growth factor receptor, leading to the loading of the small G protein Ras with GTP. Following this activation step, Ras binds to and activates the kinase Raf, which stimulates a kinase cascade culminating in the phosphorylation of ERK. The PI3K/Akt pathway (hereafter the Akt pathway) is generally activated by the binding of the regulatory p85 subunit to tyrosine-phosphorylated sites on growth factor receptors or on associated adaptor proteins such as IRS-1 or Gab1. This binding leads to activation of the associated p110 catalytic domain, which phosphorylates PIP2 in the plasma membrane to generate PIP3. Akt contains a pleckstrin homology (PH) domain, which binds to PIP3 and enables recruitment of Akt to the membrane, where it is phosphorylated by another PH-domain containing protein kinase, PDK1.

Cellular proliferation is dependent on both growth of the cell and the progression of the cell cycle to enable DNA replication, and the ERK and Akt pathways are thought to work coordinately or synergistically to stimulate both processes. Both pathways are involved in the activation of mTOR, which controls the rate of cellular growth by regulating protein translation (Manning 2004); Myc, a key

transcription factor controlling both metabolism and cell cycle (Sears, Nuckolls et al. 2000); and cyclin D, a central regulator of the transition from G1 to S phase of the cell cycle (Mirza, Gysin et al. 2004). Other downstream effectors are specific to one of the two pathways; for example, the Akt pathway stimulates the uptake of glucose, while ERK stimulates immediate-early transcription factors including Fos and Egr1. Because the ERK and Akt pathways are both pleiotropic and highly intertwined, it is difficult to determine the quantitative contribution of each to the overall level of proliferation. Nonetheless, both phospho-Akt and phospho-ERK are frequently used as readouts of proliferative or oncogenic signaling.

However, several facets of the interplay between the ERK and Akt pathways suggest that they do not always work in concert. Akt is known to suppress ERK pathway signaling by phosphorylating Raf at an inhibitory site, Ser-259 (Rommel, Clarke et al. 1999; Zimmermann and Moelling 1999). Moreover, ERK is capable of contributing to mTOR activation, and the downstream mTOR effector S6K1 stimulates a potent negative feedback loop suppressing Akt activity (Manning 2004). Thus, the ERK and Akt pathways may also act antagonistically. These negative crosstalk pathways could play a role in maintaining a proper balance between the output of each pathway, preventing hyperactivation that might lead to uncontrolled proliferation. However, much more work is needed to understand how the dynamic interplay between these pathways leads to controlled proliferation, what combinations of signals constitute pathological or deregulated states, and what mechanisms are used by the cell to detect and suppress potentially oncogenic signaling states.

An additional key family of proteins in cell cycle control is the cyclin-depdendent kinase inhibitors, which fall into two families: p16/19^{Arf} and the Cip/Kip family. The Cip/Kip family, consisting of p21^{Cip1}, p27^{Kip1}, and p57^{Kip2} are capable of binding to multiple Cyclin-CDK complexes and can arrest the cell cycle during G1, S, or G2 phases. These proteins may also play a critical role in cell cycle progression by acting as assembly factors for the CDK4/6-Cyclin E complex, promoting late G1 to S phase transition (LaBaer, Garrett et al. 1997). Within the context of growth factor-mediated signaling, p27 is recognized as a central regulator of the balance between quiescence and proliferation(Rivard, L'Allemain et al. 1996). Akt suppresses p27 activity by phosphorylating it and stimulating translocation to the cytoplasm, where it is degraded (Liang, Zubovitz et al. 2002). p21 is best known for its role in p53-mediated cell cycle arrest in response to DNA damage or other stresses (el-Deiry, Tokino et al. 1993; Harper, Adami et al. 1993), and has been reported to be either stimulated or suppressed by Akt, and potentially activated by the ERK pathway. Less is known about p57, although it is the only member of this family required for mouse embryonic development, and is important in differentiation (Yan, Frisen et al. 1997).

In this study, we identify p57 as an effector of regulatory crosstalk between the ERK and Akt pathways; activation of the Akt pathway stimulates p57 expression, while the ERK pathway suppresses it. This cross-regulatory motif plays a key role in determining the proliferative response of mammary epithelial cells to IGF-1/insulin and EGF. Activation of the PI3K pathway in the absence of ERK activity, either by IGF-1/insulin or by mutant PI3K isoforms, leads to upregulation of p57 and proliferative arrest. Depletion of p57 reverses this arrest, enabling IGF-1-induced proliferation in the absence of EGF and greatly enhancing proliferation of cells harboring PI3K mutations. Thus, regulation of p57 by ERK and Akt acts as a network sensor capable of detecting and limiting the proliferative response to "imbalanced" signaling situations in which the PI3K/Akt is activated in isolation from other pathways.

Results

MCF-10A cells are typically cultured in growth medium containing both insulin and EGF (with insulin present at very high concentrations capable of stimulating the IGF-1 receptor). To examine the contribution of these mitogens to proliferative behavior, we cultured MCF-10A cells under various concentrations of EGF and IGF-1 and assessed proliferation by staining for phosphorylated

retinoblastoma protein (pRb), an indicator of cell cycle progression. As expected, very few cells (15%) were pRb-positive in the absence of both EGF and insulin, while the highest level of pRb staining (82%) was observed at maximal levels of both EGF and insulin (Figure 1A). While EGF alone was capable of stimulating proliferation in a dose-dependent manner, IGF-1 alone had a limited effect, even at saturating concentrations. At sub-maximal levels of EGF, co-stimulation with IGF-1 displayed a cooperative effect, increasing the pRb positive population from 25% to 50%. Thus, both EGF and insulin transduce proliferative signals, but those downstream of insulin require additional input from the EGF-stimulated network.

In agreement with previous work, EGF potently stimulated phosphorylation of ERK, but stimulated the Akt pathway relatively weakly as indicated by frequent nuclear localization of FOXO3a (Figure 1B). In contrast, insulin strongly induced PI3K/Akt activity leading to widespread cytoplasmic localization of Foxo3a, but induced pERK at levels 10-fold lower than EGF.

To examine the signals contributing to proliferation downstream of EGF and IGF-1, we measured a panel of 15 proliferation-related protein signals by HTIF (Fig. 1C). As expected, numerous signals downstream of both ERK and Akt, including c-Myc, Fra-1, and phospho-S6, displayed activation by both EGF and IGF-1. However, the cell cycle regulators $p21^{Cip1}$ and $p57^{Kip2}$ displayed a unique pattern of regulation: expression of these two proteins increased in response to IGF-1 but not EGF. Conversely, expression of p27 was suppressed by EGF, but did not change in response to IGF-1. A more detailed analysis of p21 and p57 dynamics revealed a key difference: while both proteins were induced under stimulation by IGF-1 alone, p57 levels were suppressed by co-treatment with EGF (Fig. 2A-C). This suppression was not observed with p21, which was expressed at similar levels regardless of EGF. At the single-cell level, both p21 and p57 expression were present primarily in pRb-negative cells, confirming that both proteins are acting in an anti-proliferative role (Fig. 2D).

We therefore asked whether activation of p21 or p57 were involved in suppression of proliferation in response to IGF-1. p57 was depleted in MCF-10A cells using 3 separate shRNA constructs (Fig. 3A,C). Relative to control shRNA construct or uninfected cells, depletion of p57 induced a general increase in the fraction of pRb-positive cells (Fig. 3B). To determine whether p57 played a specific role in insulin-stimulated proliferation, we examined the ratio of pRb-positive cells in insulin-stimulated cells relative to cells cultured in the absence of growth factors. This ratio was increased 3 to 6 fold in p57 knockdown cells (Fig. 3D), indicating that p57 is capable of specifically suppressing insulin/IGF-1-induced proliferation. In contrast, no such enhancement of the insulin-stimulated proliferation was observed in p21 +/- or p21-/- MCF-10A cells (Karakas, Weeraratna et al. 2006). Thus, p57 but not p21 appears to be involved in limiting IGF-1/insulin-mediated proliferation. We therefore focused on the regulation of p57 by IGF-1 and EGF.

Because insulin activates the PI3K/Akt pathway more strongly than does EGF, we examined whether this pathway was involved in regulation of p57 expression. Small molecule inhibitors of either PI3K activity or mTor kinase activity reduced insulin-mediated p57 expression by ~3-fold, returning it to near basal levels (Figure 4A,B). In contrast, only a modest change was observed under rapamycin treatment, which specifically targets mTORC1. Furthermore, using computational analysis of single-cell data, we found that p57 expression was correlated with higher levels of pAkt in individual cells (Fig. 4E). Thus, the PI3K/Akt pathway appears to be involved in upregulating p57 expression. To examine whether Akt activity alone is sufficient to induce p57 expression, we made use of an inducible Akt construct that can be selectively activated by treatment with 4-hydroxy tamoxifen (4OHT) (Kohn, Barthel et al. 1998). Cells expressing myrAkt-ER were first cultured for 48 hours in the absence of growth factors to eliminate all other signals, and then stimulated with 4OHT at various time points prior to fixation. Expression of p57 increased 2-fold within 4 hours of treatment, and reached 10-fold after 24 hours (Fig. 4C). In contrast, treatment with 4OHT in the presence of EGF failed to induce a significant increase in p57 (Fig.

4D). Therefore, activation of Akt alone is sufficient to induce p57 expression, which can be suppressed by a pathway downstream of EGF. Using RT-PCR, we found that p57 mRNA was upregulated 1.5-fold by insulin treatment and suppressed 2 to 3-fold by treatment with PIK-90, suggesting that the regulation of p57 by the PI3K pathway occurs at least partly at the transcriptional level.

EGF is a potent activator of the ERK signaling pathway, and we therefore tested whether ERK activity was involved in suppressing p57 expression. Treatment of EGF-stimulated cells with the MEK inhibitor PD98059 led to a 2.2-fold increase in the expression of p57, indicating that this pathway is indeed required for EGF-mediated downregulation of p57. Additionally, we found that overexpression of Ras^{V12} or MEK2DD, constitutive activators of ERK, resulted in suppression of insulin-stimulated p57 induction.

The ability of p57 to limit IGF-1-driven proliferation suggests that it may be a suppressor of oncogenic signaling through the PI3K pathway. To test this hypothesis, we made use of MCF-10A cells in which frequently occurring oncogenic mutations of the PIK3CA gene (E545K or H1047R) have been stably integrated at the genomic PIK3CA locus (Gustin, Karakas et al. 2009). As previously reported, both mutations conferred moderate proliferative activity in the absence of EGF. Under these conditions, p57 expression was high, consistent with our previous findings that PI3K activity in the absence of EGF leads to p57 upregulation. Strikingly, the EGF-independent proliferation of the mutant cells was enhanced 5-10 fold by shRNA-mediated depletion of p57 (Fig. 6A,B).

Furthermore, we noted that EGF-independent proliferation of PI3K mutant MCF10A cells was potently blocked by the EGFR antagonist antibody C225, suggesting that autocrine signaling through the EGF receptor is essential for proliferation (Fig 6B,C). In support of this conclusion, we noted that pS6, a signal induced uniformly across the entire population by treatment with exogenous EGF, was activated heterogeneously within the population in the absence of EGF, with isolated clusters of neighboring cells sharing high levels of signaling. However, even in the presence of C225, depletion of p57 resulted in a 10-fold increase in the percentage of pRb-positive cells (Fig. 6C). Thus, PIK3CA mutant cells require autocrine EGF signaling for proliferation, but this requirement can be bypassed by p57 depletion.

We next assessed the effect of p57 depletion in a 3-dimensional *in vitro* model of cellular transformation (Debnath, Mills et al. 2002). Relative to control shRNA constructs, p57 depletion resulted in an ~2-fold increase in the size of acini formed in 3D by MCF-10A cells (Fig. 7A,C), which was accompanied by a marked increase in the number of cells pRb cells within the acini (Fig. 7B). Thus, p57 plays a key role in growth arrest in 3D as well as monolayer culture.

Discussion

We demonstrate a novel mechanism by which ERK and Akt signals are integrated in the control of cellular proliferation. Activation of Akt is sufficient to stimulate p57 expression in mammary epithelial cells, and is required for the insulin-stimulated upregulation of p57. In contrast, ERK activation is required for the EGF-mediated suppression of p57 levels. Previous work has identified numerous integration points between the ERK and Akt pathways, including cyclin D1, c-Myc, and mTOR, but in these pathways, the integrator responds positively to both ERK and Akt signals (REF). In contrast, the mechanism reported here is unique in that one pathway (ERK) is required to negate the anti-proliferative function of the other (Akt).

One potential explanation for this signaling motif is that it serves as a sensor for imbalanced or oncogenic signaling. Many cancers display activation of the PI3K network via mutations in the catalytic subunit of PI3K or loss of PTEN. These mutations promote aberrant cell survival and proliferation, and it would be beneficial for the cell to be able to distinguish between "normal" signaling, in which multiple pathways are engaged by an activated receptor tyrosine kinase binding to its ligand, from oncogene-stimulated

4

signaling, in which a smaller subset of signaling pathways are hyperactivated due to an oncogenic mutation. The motif described here may play such a role by inducing a potent cell-cycle inhibitor in response to a signaling pattern biased toward the PI3K/Akt network, which is suppressed by ERK during normal EGF-stimulated proliferation. This hypothesis would suggest that this barrier imposed by p57 would need to be overcome at some point in the progression of tumors driven by PI3K network hyperactivation, and indeed, many breast cancers display a loss of p57 expression due to histone methylation (Yang, Karuturi et al. 2009). Moreover, such a barrier could impose a selective pressure for additional mutations capable of activating the ERK pathway, which could contribute to the appearance of co-existing mutations in the PI3K and ERK pathways, which are found in many tumors (Halilovic, She et al.). A careful bioinformatic study of the mutational status of these pathways in conjunction with p57 expression status will be necessary to evaluate this hypothesis.

A major challenge in signal transduction research is to understand how complex networks integrate multiple signals to arrive at a phenotypic cell fate decision. A number of computational models have been developed that are capable of predicting the levels and kinetics of ERK and Akt activation in response to receptor activation or pharmacological inhibition (refs.). However, the connections downstream of ERK and Akt that determine cell cycle control and proliferative outcome have yet to be extensively modeled. Developing a quantitative understanding of the connection between upstream signals and downstream phenotypes will be essential for predicting the efficacy of inhibitors targeted toward these pathways, and these models will depend on accurate "wiring diagrams" of the multiple integration points between ERK and Akt pathway effectors. The mechanism described here adds to the list of known integration points; additional studies will be needed to understand the relative importance of the various integration mechanisms, which will likely be highly context-dependent.

Materials and Methods

Abbreviations. cyclin-dependent kinase (CDK), cyclin-dependent kinase inhibitor (CKI), Mitogen Activated Protein Kinase (MAPK), Extracellular Signal-regulated Kinase (Borisov, Aksamitiene et al.), Phosphoinositide 3-Kinase (PI3-Kinase, PI3K), Epidermal Growth Factor (EGF), myristoylated-Akt (myr-Akt),

Reagents. Primary Antibodies: anti-p21 (rabbit-2947 Cell Signaling, mouse-556430 BD Biosciences), anti-p27 (rabbit-36865 Cell Signaling, mouse-610241BD Biosciences), anti-p57 (rabbit-2557 Cell Signaling, mouse monoclonal-SC56341 Santa Cruz), anti-phospho-ERK (rabbit-4370L Cell Signaling), antiphospho-Rb-S780 (mouse-55835 BD Biosciences, goat polyclonal-SC12901 Santa Cruz), phospho-S6 (rabbit-4858L Cell Signaling) phospho-Akt-S473 (rabbit-4060L Cell Signaling). Dual Antibodies (Cell Signaling): p-S6 Ribosomal Protein (S2351236) (D57.2.2E) (Alexa®647)-rabbit-mAb-4851B, p-Rb (S807/811) (Alexa®555)-rabbit-Ab-3937B. Secondary Antibodies (Invitrogen): Alexa fluor 488 (donkey-anti-mouse-A21202, goat-anti-mouse-A11029, goatanti-rat-A11006), Alexa fluor 555 (donkey-anti-rabbit-A31572, goat-anti-rabbit-A21429), Alexa fluor 647 (donkey-anti-goat-A21447, goat-anti-mouse-A21236). Inhibitors: DMSO (Sigma D2650), PIK90 (Axon-1362), PD98059 (Calbiochem-513000), Torin-1 (Nathanael Gray), GSK3 Inhibitor X (Calbiochem-361551), GSK3 Inhibitor XV (Calbiochem-361558).

Cell Culture. MCF-10A Mammary Epithelial Cells (Soule et al., 1990) were obtained from American Type Culture Collection and cultured, as previously described (Debnath et al. 2003), in DMEM/F12 (Invitrogen) supplemented with 5% horse serum, 20 ng/ml EGF, 10 μg/ml insulin, 0.5 μg/ml hydrocortisone, 100 ng/ml cholera toxin, 50 U/ml penicillin, and 50 μg/ml streptomycin. In experiments where the concentration of growth factors varies, the corresponding concentration of EGF and insulin were added to MCF-10A Assay Medium (see Debnath et al., 2003), containing the supplements above in the absence of EGF or insulin. T98G Hepatocarcinoma Cells were obtained from XX and cultured in

DMEM supplemented with 10% fetal bovine serum, 1% L-glutamine, 50 U/ml penicillin, and 50 μg/ml streptomycin.

Continuous-growth assay. To simulate continuous cell growth and division from time of plating, MCF-10A cells were plated at 10,000 cells/well in a 96-well plate and cultured for 24h in full MCF-10A growth medium. After 24h, cells were washed 1x with PBS and growth conditions were changed to those indicated for the experiment. Cells were then grown for 24h, fixed, and stained according to Immunofluorescence Staining.

Quiescence-release assay. To simulate conditions of quiescence release into growth, MCF-10A cells were plated at 10,000 cells/well in a 96-well plate and cultured for 24h in full MCF-10A growth medium. After 24h, cells were washed 1x with PBS and MCF-10A Assay Medium was added. 48h after conditions were changed to Assay Medium, growth conditions were changed to chose indicated for the experiment. Cells were then grown for 24h, fixed, and stained according to Immunofluorescence Staining.

Immunofluorescence Staining. Attached cells growing in monolayer culture were fixed using 1.8-2% paraformaldehyde (PFA) in 1% PBS for 15 minutes at room temperature. Following fixation, cells were permeabilized with methanol and washed once with PBS-Tween (PBS-T) buffer (5% Tween). Blocking was performed by addition of Odyssey Blocking Buffer (OBB) for 30 minutes at room temperature. Primary antibodies were incubated at 1:100 dilutions in OBB for sixty minutes at room temperature and then washed three times with PBS-T. Secondary antibodies were diluted in OBB as follows (p-S6-667 1:10, p-Rb-555 1:100, all others 1:250) and incubated at room temperature for sixty minutes. Cells were washed twice with PBS-T. Nuclei were stained with DAPI diluted 1:2000 and whole cells were stained with WCS Blue diluted 1:500 in PBS for thirty minutes at room temperature. Cells were washed twice with PBS and maintained in PBS for imaging using a CellWorx Scanner.

Immunofluorescence Analysis. 3-4 image fields were collected for each channel in each well of a 96 well plate (uniform count per experiment). Wavelength channels imaged include A350 (350nm for DAPI/WCS Blue stain), 488nm, Cy3 (555nm), and Cy5 (647nm). TIFF images were processed using ImageRail (Bjorn Millard) by cell segmentation using the DAPI nuclear threshold pixel value, the WCS Blue cytoplasmic threshold pixel value, and extrapolating cytoplasmic range by measuring pixel values within an annulus of 5 pixels radial to the nucleus. Thresholds set were slightly variable between 96 well plates, but common threshold values are: nucleus: 500, cytoplasm: 100. Inspection of cell segmentation revealed successful identification of nuclei for greater than 90% of cells. For the <10% cells that were not correctly identified, the majority of errors resulted from repetition of nuclei, not failure to differentiate between two nuclei. Immunofluorescence levels were recorded for single cells in each field of the plate and exported into a Microsoft Excel file.

Data were then converted into histograms using Matlab (Matlab version R2009a). Mean nuclear or cytoplasmic fluorescence values were separated into 100 evenly spaced bins. Histograms were generated by plotting relative fluorescence versus number of cells per bin while normalizing for total cell number. p-Rb percentage was calculated by identifying the threshold value

Cell density plots were generated by plotting the relative intensity of fluorescence A versus the relative intensity of fluorescence B and separating each into 100 evenly spaced bins. A color scale ranging from blue to red was used to represent low to high cell density.

RT-PCR. Attached cells growing in monolayer were washed 2x with PBS. 2ml TRIzol reagent was added per well in a 6-well plate and pipetted up and down to ensure sample homogenization. After 5min incubation at RT, 1ml sample transferred to Eppendorf tube.

References

Borisov, N., E. Aksamitiene, et al. (2009). "Systems-level interactions between insulin-EGF networks amplify mitogenic signaling." Mol Syst Biol **5**: 256.

Debnath, J., K. R. Mills, et al. (2002). "The role of apoptosis in creating and maintaining luminal space within normal and oncogene-expressing mammary acini." Cell **111**(1): 29-40.

el-Deiry, W. S., T. Tokino, et al. (1993). "WAF1, a potential mediator of p53 tumor suppression." Cell **75**(4): 817-25.

Gustin, J. P., B. Karakas, et al. (2009). "Knockin of mutant PIK3CA activates multiple oncogenic pathways." Proc Natl Acad Sci U S A **106**(8): 2835-40.

Halilovic, E., Q. B. She, et al. "PIK3CA mutation uncouples tumor growth and cyclin D1 regulation from MEK/ERK and mutant KRAS signaling." Cancer Res **70**(17): 6804-14.

Harper, J. W., G. R. Adami, et al. (1993). "The p21 Cdk-interacting protein Cip1 is a potent inhibitor of G1 cyclin-dependent kinases." Cell **75**(4): 805-16.

Karakas, B., A. Weeraratna, et al. (2006). "Interleukin-1 alpha mediates the growth proliferative effects of transforming growth factor-beta in p21 null MCF-10A human mammary epithelial cells." Oncogene **25**(40): 5561-9.

Kohn, A. D., A. Barthel, et al. (1998). "Construction and characterization of a conditionally active version of the serine/threonine kinase Akt." J Biol Chem **273**(19): 11937-43.

LaBaer, J., M. D. Garrett, et al. (1997). "New functional activities for the p21 family of CDK inhibitors." Genes Dev **11**(7): 847-62.

Liang, J., J. Zubovitz, et al. (2002). "PKB/Akt phosphorylates p27, impairs nuclear import of p27 and opposes p27-mediated G1 arrest." Nat Med **8**(10): 1153-60.

Manning, B. D. (2004). "Balancing Akt with S6K: implications for both metabolic diseases and tumorigenesis." J Cell Biol **167**(3): 399-403.

Mirza, A. M., S. Gysin, et al. (2004). "Cooperative regulation of the cell division cycle by the protein kinases RAF and AKT." Mol Cell Biol **24**(24): 10868-81.

Rivard, N., G. L'Allemain, et al. (1996). "Abrogation of p27Kip1 by cDNA antisense suppresses quiescence (G0 state) in fibroblasts." J Biol Chem **271**(31): 18337-41.

Rommel, C., B. A. Clarke, et al. (1999). "Differentiation stage-specific inhibition of the Raf-MEK-ERK pathway by Akt." Science **286**(5445): 1738-41.

Sears, R., F. Nuckolls, et al. (2000). "Multiple Ras-dependent phosphorylation pathways regulate Myc protein stability." Genes Dev **14**(19): 2501-14.

Yan, Y., J. Frisen, et al. (1997). "Ablation of the CDK inhibitor p57Kip2 results in increased apoptosis and delayed differentiation during mouse development." Genes Dev **11**(8): 973-83.

Yang, X., R. K. Karuturi, et al. (2009). "CDKN1C (p57) is a direct target of EZH2 and suppressed by multiple epigenetic mechanisms in breast cancer cells." PLoS One **4**(4): e5011.

Zimmermann, S. and K. Moelling (1999). "Phosphorylation and regulation of Raf by Akt (protein kinase B)." Science **286**(5445): 1741-4.

Figure legends

Figure 1. Differential regulation of proliferation and the PI3K and ERK pathways by IGF-1 and EGF

A. Percentage of phospho-Rb-positive cells under various culture conditions. Cells were treated with the indicated growth factors in a continuous growth format, and pRb was detected by HTIF after 24 hours

B. Stimulation of Akt, ERK, and cell cycle progression by EGF and IGF-1. MCF-10A cells were cultured for 24 hr in the presence of the growth factors indicated. Phospho-Akt, phospho-ERK, and phospho-Rb were measured by HTIF as described in Materials and Methods.

C. HTIF screen for key signaling differences between EGF and IGF-1 signaling. MCF-10A cells were cultured in the presence or absence of EGF and IGF-1, and the indicated protein signals were detected by HTIF.

Figure 2. Dynamics of p57 regulation coordinated by IGF-1 and EGF.

Figure 3. Enhancement of IGF-1-stimulated-independent proliferation in p57-depleted cells

A. Depletion of p57 by shRNA. MCF-10A cells were stably infected with a lentiviral vector expressing shRNA hairpins targeting p57 or a non-targeting control hairpin. p57 expression was measured by HTIF.

B. Proliferative response to growth factors in p57-depleted cells. Control and p57 hairpin-expressing MCF-10A cells were cultured in the presence of the indicated growth factors. Proliferation, as assessed by pRb immunofluorescence, was quantified by HTIF.

Figure 4. Upregulation of p57 expression by the PI3K/Akt/mTOR network.

A. Blockage of p57 stimulation by Inhibition of PI3K or mTOR kinase activity. MCF-10A cells were cultured in the presence of insulin (10 ug/ml) for 24 hr in the presence of the indicated inhibitors. Expression of p57 was measured by HTIF.

B. Quantitation of nuclear p57 expression by HTIF under the conditions shown in (A).

C. Correlation of pAkt and p57 signals at the single-cell level.

D. Stimulation of p57 expression in the absence of growth factors by inducible Akt. MCF-10A cells stably expressing an inducible Akt construct were cultured in the absence of growth factors for 48 hr and then stimulated with vehicle (EtOH) or inducer (4-OHT) in the presence or absence of for the indicated times, and p57 expression was measured by HTIF.

Figure 5. Downregulation of p57 expression by the Ras/Mek/ERK pathway.

A. Upregulation of p57 upon MEK inhibition. MCF-10A cells were cultured in the presence of EGF (20 ng/ml) and vehicle (DMSO) or MEK inhibitor (PD98059) For 24 hr. Expression of p57 was quantified by HTIF.

B. Suppression of p57 expression by activated mutants of MEK and Ras. MCF-10A cells stably expressing MEK-DD or RasV12 were cultured in the presence or absence of insulin for 24 hr, and p57 expression was quantified by HTIF.

C. Correlation of pErk and p57 signals at the single-cell level.

Figure 6. Cooperative enhancement of EGF-independent proliferation by PIK3CA mutation and p57 depletion.

Figure 7. Induction of hyperproliferation in 3D cell culture by p57 depletion.

Figure 1

Figure 2

A

EGF (ng/ml)
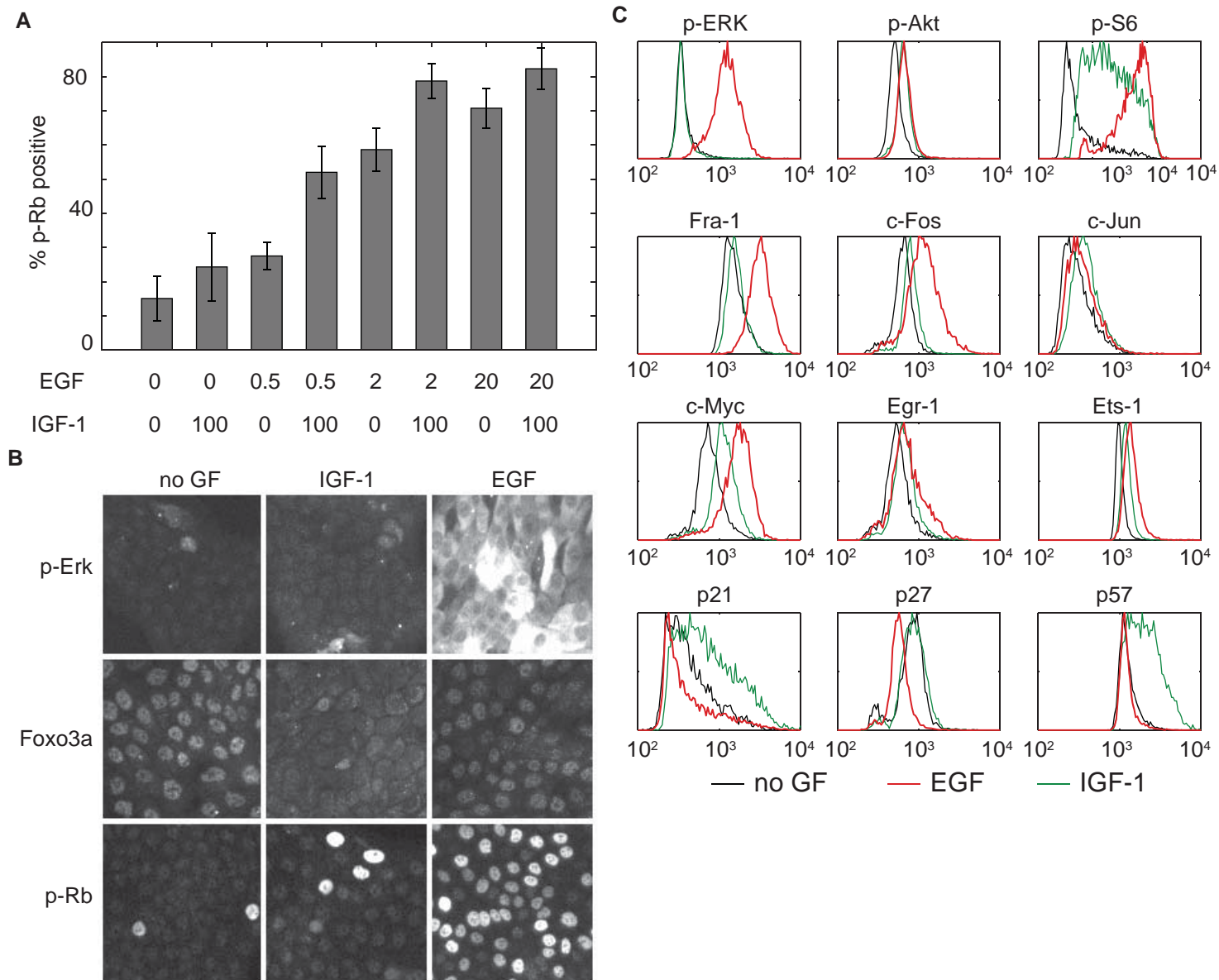
0   0.5   2   20

-ins

+ins

High

p57

Low

B

EGF (ng/ml)

0   0.5   2   20

freq.

1

0

p57 level   p57 level   p57 level   p57 level

—— -ins
—— +ins

C

p57 (a.u.)

180

0

0   0.5   2   20

EGF (ng/ml)

■ -ins
■ +ins

D

pRb

2.5
2.4
2.3
2.2
2.1
2
1.9
1.8
1.7

2   2.5   3   3.5

p57

Figure 3

A

| uninf. | NT | p57-A | p57-B | p57-C |

High

p57

Low

B

-ins

+ins

Blue: DAPI

Red: pRb

C

freq.

p57 level

— uninf.
— NT
— p57-A
— p57-B
— p57-C

D

pRb induction by ins

uninf.   NT   p57-A   p57-B   p57-C

Figure 4

A

+ insulin

DMSO   PIK-90   Torin-1   Rapamycin

High

p57

Low

B

— ins + DMSO
— ins + PIK-90
— ins + Torin-1
— ins + Rapamycin

C

2 hr   4 hr   6 hr

D

E

F

| PIK-90 | - | + | - | + |
| ins | - | - | + | + |

Figure 5

A

| EGF (ng/ml) | 0 | 0 | 20 | 20 | 0 | 0 | 20 | 20 |
| INSULIN (µg/ml) | 0 | 10 | 0 | 10 | 0 | 10 | 0 | 10 |

DMSO

p57

PD98059

Fluorescence Intensity

p57

B

Cell Line	pBabe-puro	MEKDD	RasV12	pBabe-puro	MEKDD	RasV12
EGF (ng/ml)	0	0	0	0	0	0
INSULIN (µg/ml)	0	0	0	10	10	10

p57

Fluorescence Intensity

C

Figure 6

A

MCF10A-E545K

| non-targeting | p57 sh-A | p57 sh-B |

MCF10A-H1047R

| non-targeting | p57 sh-A | p57 sh-B |

no GF

no GF +C225

Blue: DAPI

Red: pRb

B

no growth factor

C

no growth factor +C225

Figure 7

A
non-targeting   p57 sh-A   p57 sh-B

B

C

percentage of acini per size

90
80
70
60
50
40
30
20
10
0

< 0.4   0.4-0.8   0.8-1   > 1
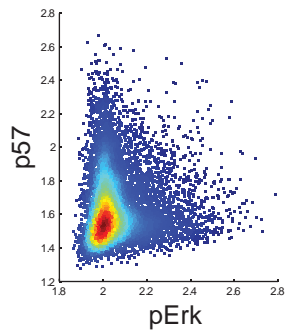
acinar size distribution
(bins with arb. units)

vector
p27_B5_sh
p57_B2_sh
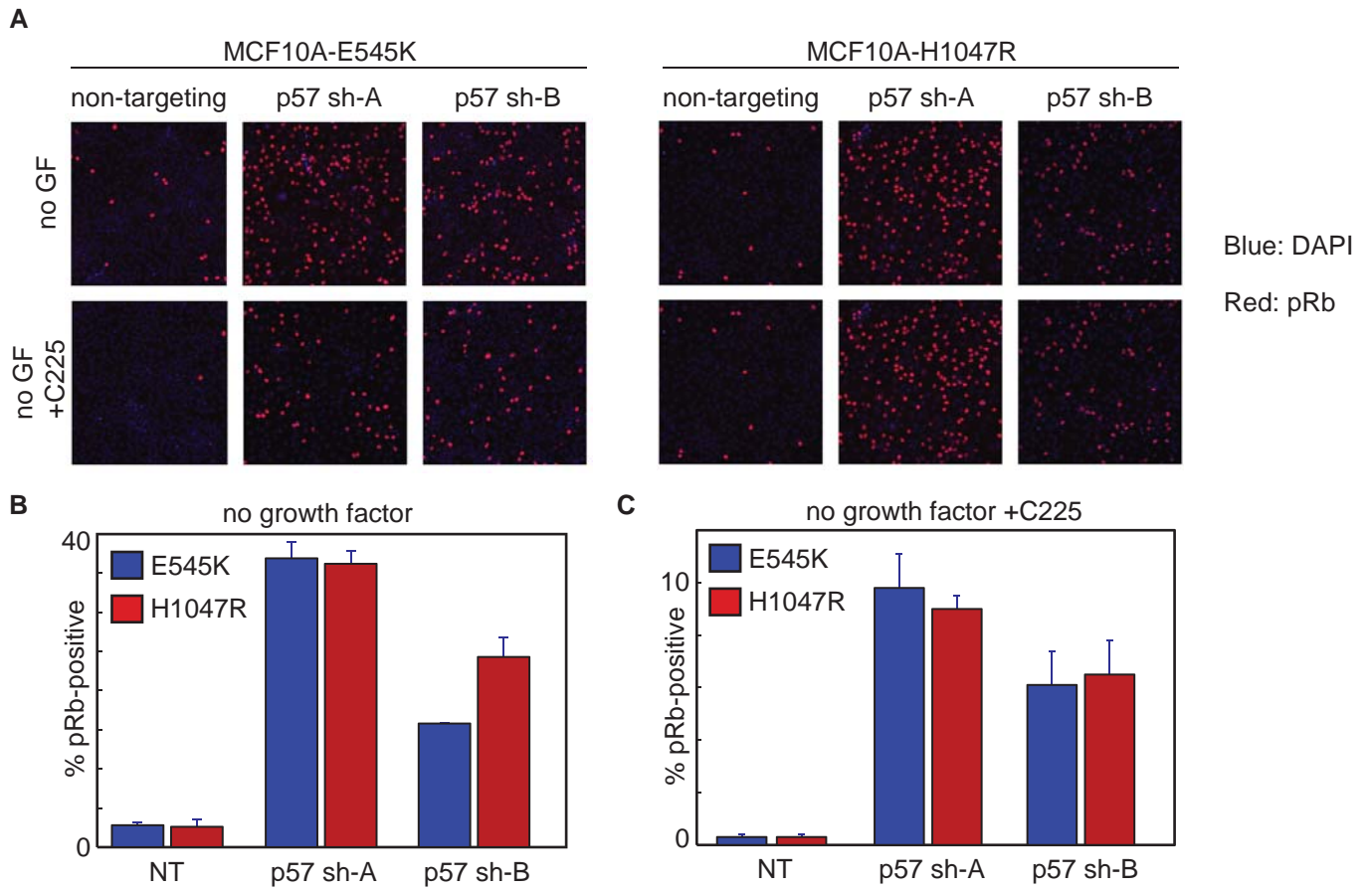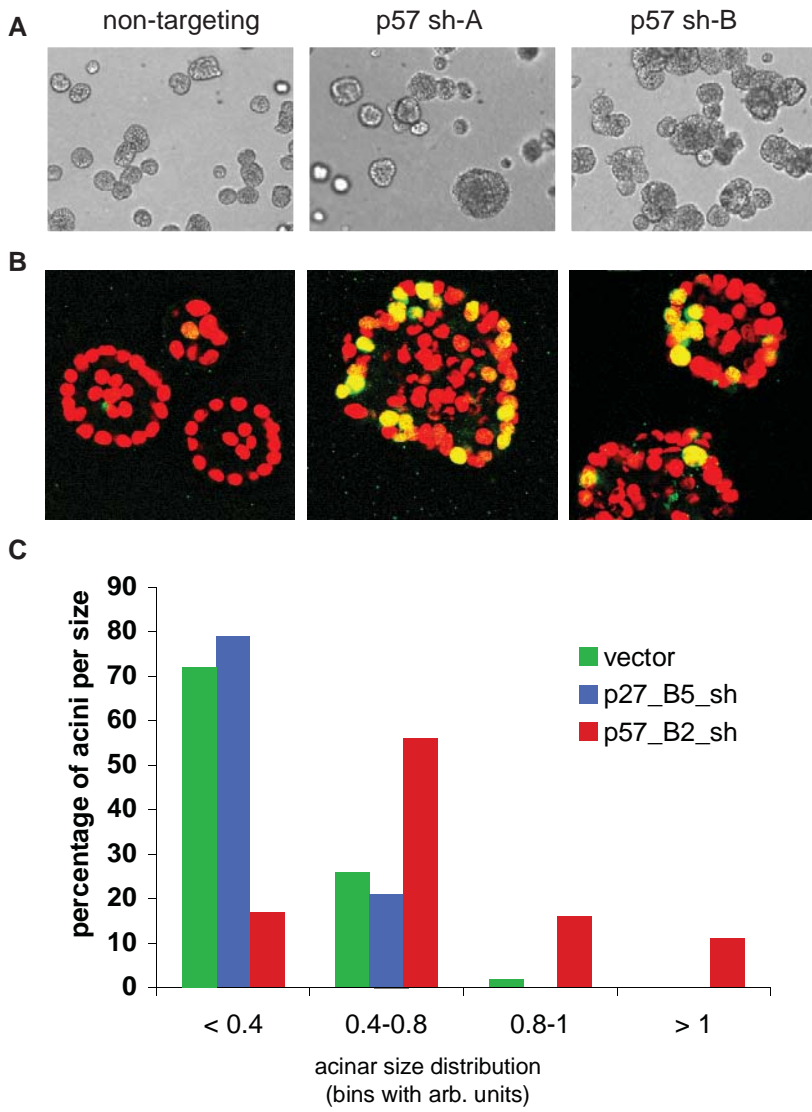
p57Kip2 expression is stimulated by the PI3K/Akt pathway and acts as a detector of imbalanced oncogenic signaling

Devin Worster[1], John Albeck[1], Bjorn Millard[2], Gordon Mills[3], Joan Brugge[1]

[1] Department of Cell Biology, Harvard Medical School

[2] Department of Systems Biology, Harvard Medical School

[3] Department of Systems Biology, University of Texas M.D. Anderson Cancer Center

Proliferation of mammary epithelial cells is stimulated by epidermal growth factor (EGF), but not by insulin-like growth factor 1 (IGF-1) or insulin. To understand the signaling mechanisms underlying this difference, we examined a panel of 15 growth-related signaling proteins at the single-cell level using automated high-content immunofluorescence microscopy. This analysis revealed that the cell cycle inhibitor p57^{Kip2} is highly expressed under conditions of insulin stimulation, but not under EGF. Using a combination of pathway-specific inhibitors and activated signaling proteins, we show that p57^{Kip2} is potently activated by Akt activity, but strongly repressed by Erk activity. Depletion of p57^{Kip2} enables proliferation in response to insulin alone. Thus, p57^{Kip2} is capable of sensing the ratio of Erk- to Akt-mediated signals and arresting cell growth when this ratio is too high. Interestingly, expression of oncogenes such as ErbB2 or myrAkt that favor activation of the PI3K/Akt pathway induce p57^{Kip2} expression, while oncogenes such as Ras that favor activation of the Erk pathway do not. Our results offer a potential explanation for the finding that the p57^{Kip2} locus is silenced in many breast cancers, which frequently show hyperactivation of the PI3K pathway. The expression status of p57^{Kip2} may be an important factor to assess when considering targeted therapy against the Erk or PI3K pathways.